INVESTIGATION OF RC WALL FAILURE MECHANISMS USING NONLINEAR CONTINUUM ANALYSIS

Z. Whitman [(1)], L.N. Lowes [(2)], D.E. Lehman [(3)]

[(1)] *Engineer, Coughman, Porter, Lundeen, Seattle, WA, USA,*
[(2)] *Professor, Dept. of Civil and Env. Engineering, University of Washington, Seattle, USA, lowes@uw.edu*
[(3)] *Professor, Dept. of Civil and Env Engineering, University of Washington, Seattle, USA, delehman@uw.edu*

Abstract

The research presented here employed nonlinear continuum analysis to investigate the design parameters that determine the failure mechanism and deformation capacity of planar and nonplanar reinforced concrete walls. Several commonly used finite element software packages were investigated for use in nonlinear analysis of concrete walls; the ATENA software package (www.cervenka.cz) was found to best meet the requirements of accuracy, numerical efficiency and robustness, as well as ease of use. One of the most important properties was the automated regularization of concrete material response in compression. Regularization of concrete compression response is required to achieve accurate and mesh-objective simulation of wall failure, which often results from concrete crushing. In ATENA, regularization is a function of a user-defined deformation at compression failure, which is approximately linearly related to the energy dissipated during concrete crushing. The modeling approach was validated through comparison of simulated and observed response for a suite of planar and nonplanar concrete walls subjected to lateral and axial loading in the laboratory. Results show that strength and drift capacity can be predicted with a high level of accuracy. Using the validated numerical model, the impact of various design parameters on failure mechanism and drift capacity were investigated. Results show that walls subjected to high shear demands and/or with large length-to-thickness ratios exhibit a more brittle compression-shear failure, while walls with lower shear demands and smaller length-to-thickness ratios exhibit more ductile compression- or tension-controlled flexural failures.

Keywords: reinforced concrete; wall; flexural wall; nonlinear analysis; finite element analysis

1. Introduction

Slender reinforced concrete walls are used commonly as the lateral load resisting systems in mid- and high-rise buildings in regions of high seismicity. Walls provide significant stiffness to meet drift limits, provide significant strength to meet design-level strength requirements, and are easily configured to meet architectural requirements. Walls with height to length ratios in excess of 2.0 are typically considered to be slender and are expected to exhibit flexure-controlled response, with strength determined by yielding of longitudinal steel and deformation capacity determined by either low-cycle fatigue fracture of longitudinal steel or compression failure of the boundary element.

Figure 1 shows an idealized reinforcing steel layout that is typical of a planar wall in a modern mid-rise building in the US. Longitudinal reinforcement is concentrated in well-confined boundary elements at the ends of the wall and the web region of the wall has a relatively low longitudinal reinforcement ratio. Horizontal reinforcement in the web is designed to carry the shear load; often shear capacity approaches the ACI Code maximum of $10\sqrt{f_c'}A_g$. Finally, the wall cross-sectional aspect ratio (ratio of wall length to thickness) is large, typically in excess of 20 [1].

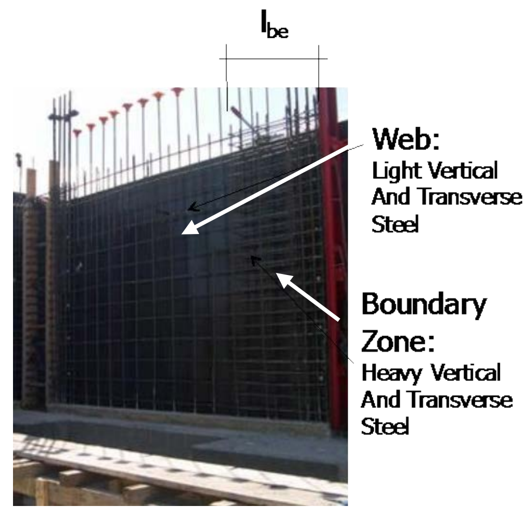

Figure 1: Typical reinforcement layout

To improve understanding of the earthquake response of slender walls, Birely [1] reviewed data from 43 laboratory tests of planar walls and post-earthquake reconnaissance data for 23 earthquakes. On the basis of this review, Birely [1] concluded that slender walls typically exhibit one of three failure mechanism: buckling-rupture (BR) characterized by fracture of previously buckled longitudinal reinforcement, compression-buckling (CB) characterized by simultaneous concrete crushing and reinforcement buckling in the boundary element or compression-shear (CS) characterized by crushing of boundary element and web-region concrete. Birely found also that for walls exhibiting flexural response, drift capacity is determined primarily by shear stress demand and cross-sectional aspect ratio; axial load ratio has a much less significant impact (Figure 2). However, past test specimens (Table 1) shows that in comparison to walls in buildings, laboratory tests specimens have smaller cross-sectional aspect ratios and shear stress demands and lower axial load ratios than typically observed in design. Thus, the data in Tables 1 and Figure 2 bring into question the deformation capacity of typical walls in buildings.

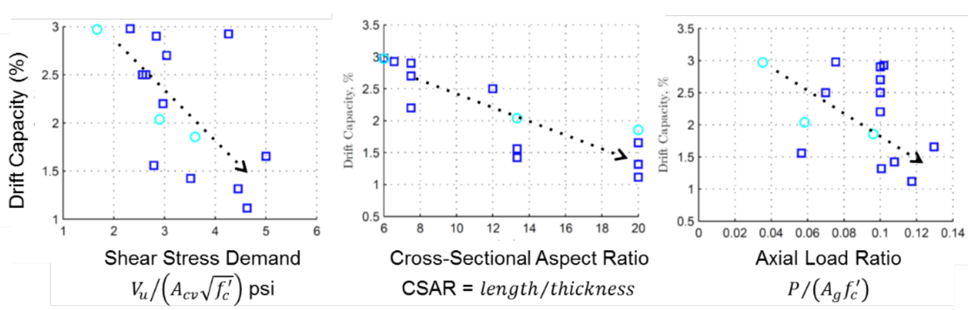

Figure 2: Drift capacity of planar wall test specimens versus design parameters
(circles indicate BR failure and squares indicate CB failure)

Questions about the drift capacity and failure mechanisms exhibited by modern walls could be answered through additional laboratory tests. However, large scale testing of specimens that are longer and sustain high shear stresses results in the need to apply large forces. This testing is very expensive as it requires a large laboratory space, high-strength actuators, and a strong reaction frame. To expand the experimental data to reflect the geometries and shear stress demand of modern walls in buildings, a parametric study was conducted using a validated nonlinear high-resolution finite element analysis. The following sections provide a summary of the process used to select the software, develop and validate the model, and the results of the parametric study. Additional information may be found in the report by Whitman [2].

Several commercial and research software packages were evaluated through comparison of simulated and measured response for a series of reinforced concrete components [2,3]. Issues considered in the evaluation included i) accuracy in prediction of strength and deformation capacity, ii) ease of use with respect to model building and extracting and visualizing simulation data, and iii) computational demand. Ultimately, the ATENA (www.cervenka.cz) software package was identified as the preferred software for the project. Existing experimental data were used to calibrate critical model parameters and validate the model for prediction of wall stiffness, strength, deformation capacity and failure mechanism; the validated models was used to expand the experimental data set and provide insight into the impact of design parameters on response mechanisms and deformation capacity.

2. Experimental Data Used for Model Calibration and Validation

A dataset comprising 23 previously tested rectangular slender wall specimens was used to calibrate and validate the continuum modeling approach employed in this study. Wall specimens were included in the data set if i) the specimen was planar (rectangular) and subjected to in-plane flexure, shear and axial loading, ii) specimens were constructed of normal weight concrete and normal strength concrete and steel, iii) specimen failure resulted from deteriorating flexural response, including bar fracture or concrete crushing and bar buckling, iv) wall specimen thickness exceeded 76 mm (3 in.), v) data required to fully define and evaluate a numerical model were provided. Table 1 lists the specimens and provides design parameters of particular interest this study. Whitman [3] provides detailed information about specimen material properties, geometric configuration, and design parameters: parameters listed in Table 1 are defined as follows:

- Cross-Sectional Aspect Ratio (CSAR) = l_w/t_w, where l_w is the wall length and t_w is the wall thickness.
- Shear span ratio = $M/(Vl_w)$, where M is the moment developed at the base of the wall, V is the shear developed at the base of the wall and l_w is the length of the wall. Note that the shear span ratio equals the vertical aspect ratio if zero moment is applied at the top of the wall.
- Axial load ratio = $P/(A_g f'_c)$, where P is the axial load at the base of the wall (including self-weight of the specimen computed assuming a unit weight of 23.6 kPa (150 lb/ft^3)), A_g is the gross area of the wall and f'_c is the measured concrete compressive strength.
- Shear stress demand = V_b / $A_{cv}\sqrt{f'_c}$, where V_b is the maximum base shear developed during the test, A_{cv} is the shear area, taken equal to $5/6A_g$ for a rectangular section, and f'_c is the concrete compressive strength in the specified units.
- Shear demand-capacity ratio = V_b/V_n, where V_b is the maximum base shear and V_n is the shear strength computed per ACI 318 [4] using measured concrete and steel strengths.
- Flexural strength ratio = M_b/M_n, where M_b is the maximum base moment developed during the test and M_n is the nominal flexural strength of the wall corresponding to a compressive strain of 0.003 at the extreme fiber using measured concrete and steel strengths.
- Δ_u = drift capacity which is the drift at which the lateral load carrying capacity of the wall dropped to 80% of the maximum, for drift demands larger than drift corresponding the maximum strength.
- Failure mode (FM) indicates the primary mechanism causing loss of lateral load carrying capacity: concrete crushing and buckling of longitudinal steel (CB), buckling followed by rupture of longitudinal steel (BR), or concrete crushing at the boundary element-web interface due to flexure-shear interaction (CS).
- Boundary element detailing (BE) indicates that boundary element confining reinforcement meets the ACI 318-14 Code requirements for a special structural wall (SBE), an ordinary structural wall (OBE) or neither (NBE).

Table 1: Wall Test Specimens Used for Model Calibration and Validation

Specimen	Reference	CSAR	Shear Span	ALR	$V_b/A_{cv}f_c$		V_b/V_n	M_b/M_n	Δu	FM	BE
				%	MPa	psi			%		
WSH1	Dazio et al. [5]	13.3	2.3	5.5	0.17	2.01	0.44	1.03	1.04	BR	NBE
WSH2		13.3	2.3	6.3	0.19	2.27	0.53	1.12	1.75	BR	NBE
WSH3		13.3	2.3	6.4	0.24	2.92	0.67	1.10	2.07	BR	OBE
WSH4		13.3	2.3	6.3	0.23	2.77	0.62	1.06	1.60	CB	NBE
WSH5		13.3	2.3	13.7	0.23	2.81	0.62	1.08	1.52	BR	OBE
WSH6		13.3	2.3	11.4	0.30	3.58	0.83	1.11	2.04	CB	NBE
W1	Liu [6]	6.0	3.1	7.6	0.19	2.31	0.39	0.98	2.98	CB	OBE
W2		6.0	3.1	3.5	0.14	1.67	0.33	0.97	2.91	BR	NBE
PW4	Lowes et al. [7]	20.0	2.0	12.2	0.38	4.63	0.88	1.19	1.01	CB	SBE
RW1	Thomsen and Wallace [8]	12.0	3.1	10.5	0.21	2.57	0.50	1.07	2.26	BR	NBE
RW2		12.0	3.1	9.2	0.22	2.65	0.52	1.16	2.35	CB	NBE
S5	Vallenas et al. [9]	21.1	1.6	4.8	0.56	6.81	0.88	1.18	1.47	CS	SBE
S6		21.1	1.6	4.8	0.53	6.42	0.83	1.12	1.65	CS	SBE
WR20	Oh et al. [10]	7.5	2.0	10.4	0.25	3.00	0.76	1.11	2.82	CB	NBE
WR10		7.5	2.0	9.8	0.24	2.87	0.64	1.08	2.82	CB	OBE
WR0		7.5	2.0	10.8	0.25	2.97	0.74	1.08	2.14	CB	NBE
R1	Oesterle et al. [11]	18.8	2.4	0.0	0.09	1.10	0.23	1.17	2.52	BR	NBE
R2		18.8	2.4	0.0	0.17	2.00	0.42	1.23	3.25	BR	SBE
RW-A20-P10-S38	Tran [12]	8.0	2.0	7.3	0.30	3.60	0.81	1.26	3.14	CB	SBE
RW-A20-P10-S63		8.0	2.0	7.3	0.51	6.10	0.91	1.13	3.00	CB	SBE
RW-A15-P10-S51		8.0	1.5	7.7	0.41	4.90	0.83	1.15	3.31	CB	SBE
RW-A15-P10-S78		8.0	1.5	6.4	0.58	7.00	0.85	1.07	3.00	CB	SBE
RW-A15-P2.5-S64		8.0	1.5	1.6	0.48	5.80	0.79	0.99	3.00	CB	SBE
Mean		12.1	2.2	7.1	0.30	3.60	0.65	1.11	2.33	--	--
Standard Deviation		5.0	0.52	3.7	0.14	1.75	0.20	0.07	0.72	--	--
COV		0.41	0.24	0.52	0.49	0.49	0.31	0.06	0.31	--	--

3. Simulation of RC Wall Response Using ATENA

3.1 Overview of the ATENA Model

Following a review of commonly employed finite element analysis software [2,3], the ATENA (www.cervenka.cz) software was chosen for use in the current study. A discussion of the ATENA models, including the concrete constitutive model, follow. Specific characteristics of the ATENA software that make it well suited for investigating concrete wall response and preferable to other software included the following:

- The ATENA concrete constitutive model provides automatic regularization of material softening in both tension and compression using an element characteristic length. This minimizes mesh sensitivity resulting from localization of damage such that mesh refinement results in convergence to a unique solution. Thus, it is possible to uniquely and accurately predict the displacement at onset of strength loss.
- The ATENA concrete constitutive model simulates concrete dilation under compressive loading such that the impact of confining reinforcement is explicitly simulated and the user is not required to estimate the impact of confining reinforcement on concrete compressive response.
- The ATENA software provides robust simulation of reinforced concrete walls subjected to flexural loading, such that it is possible achieve converged solution states for the entire load history.

The concrete constitutive model is critical to accurate response simulation for reinforced concrete components. For this study, the ATENA NC2 [13] concrete model was employed. This model employs continuum damage theory with fixed or rotating cracks to defined concrete tensile response and plasticity theory with non-associated flow to define concrete compressive response. Specifically, the plasticity model employs the Menétrey and Willam [14] yield surface and the Drucker-Prager surface to define the plastic flow potential. For tension, concrete fracture energy and a mesh-dependent length are used to define the tensile post-peak stress versus cracking strain response. For compression, the concrete stress versus plastic strain curve is parabolic to maximum strength with linear softening to produce zero compressive strength a user-defined plastic *deformation*; plastic *strain* at zero compressive strength is defined as the plastic deformation divided by a mesh-dependent length.

Calibration of the NC2 model to simulate the response of concrete in a specific wall requires user input of eight material parameters. Four of these parameters are wall-defined by experimental tests and models: concrete compressive strength, f_c', tensile strength, f_t, elastic modulus, E, and concrete fracture energy, G_f. The four additional parameters are less well defined for test data. Whitman [3] conducted a calibration study using experimental data from laboratory wall tests to determine appropriate values for these four material parameters for simulation of slender wall response. Calibrated values are listed in Table 2; wall test specimens used in the calibration study are identified in Table 1.

Table 2 - Values for ATENA Concrete Constitutive Model Parameters

Concrete Model Parameter	Description	Value Range Recommended in ATENA Users Guide	Value recommended by Whitman (2015)
Plastic Deformation, w_d	Determines the plastic deformation capacity of concrete at zero compressive stress; enables material regularization in compression.	w_d = 0.025 in to 0.125 in = 0.635 mm to 3.175 mm	w_d = 0.0425 in = 1.080 mm
Beta Factor, β	Determines the extent to which concrete dilates under inelastic compression loading	β = 0 to 0.7	β = 0, values up to 0.25 may be used
Shear Retention Factor, S_F	Determines the shear stiffness of cracked concrete.	S_F = 20 to 200	S_F = 50
Tension Softening, c_{ts}	Determines the residual tensile strength of concrete.		c_{ts} = 0.00, values up to 0.01 may be used

A relatively simple reinforcing steel model was used. Boundary element longitudinal steel and confining steel are modeled using truss elements embedded in the concrete matrix with perfect bond. Web region vertical and horizontal steel was modeled as "smeared" across individual concrete elements with perfect bond. The stress-strain response of reinforcement was modeled using a phenomenological model in which the envelope to the stress-strain history is defined as either bilinear or multilinear based on coupon test data, and unload-reload response is modeled using Menegotto-Pinto curves to simulate the Bauschinger effect. Neither bar buckling nor bar fracture are modeled as ATENA does not support tracking of strain as required to determine onset of buckling and post-buckling fracture.

To reduce computational intensity and improve numerical stability, several simplifications were introduced into the model. First, to reduce computational demand, nonlinear material models and discrete boundary element reinforcement were employed only in the bottom third of the wall where significant nonlinear response was expected. In the middle third of the wall, where flexural yielding was not expected, nonlinear material models were used but all reinforcement was smeared. In the top third of the wall, where no nonlinearity was expected, elastic material models were used. Second, to enhance numerical robustness and stability, twenty percentage of the discrete longitudinal and confining reinforcement was smeared. Third, again to enhance numerical stability and robustness, a very small volume (0.1%) of *elastic* horizontal and vertical reinforcement was added in the bottom third of the wall as smeared reinforcement. Analyses were conducted to demonstrate that the above modeling methods had no discernable effect on simulated stiffness, strength or deformation capacity [3].

3.2 Determining failure mode and displacement capacity for the ATENA model

Because bar buckling was not simulated, in some cases it was necessary to post-process analysis data to determine the displacement at which onset of strength loss would be expected due to bar buckling. Post-processing was required also to determine the failure mode as compression-buckling (CB), buckling-rupture (BR) or compression-shear (CS). Following are the rules used to determine failure mode and onset of lateral strength loss. These rules employ i) "concrete crushing" to described concrete for which simulated minimum principal stress has reached or exceeded maximum compressive strength and then diminished to 30% of the maximum strength and ii) the ratio $\varepsilon_t/\varepsilon_{u,BE}$ in which ε_t is the maximum simulated tensile strain in the longitudinal reinforcement and $\varepsilon_{u,BE}$ is the measured fracture strain for the longitudinal steel. For the tests considered, $\varepsilon_t/\varepsilon_{u,BE} = \varepsilon_{lim} = 33\%$ resulted in a BR failure. This is the initial value, and so further evaluation is needed for different steel types and load histories.

- Case 1: Wall specimen strength loss in excess of 20% of maximum strength is simulated:
  - a) If $\varepsilon_t/\varepsilon_{u,BE} < \varepsilon_{lim}$, the concrete in the vicinity of the extreme compression reinforcing bar has crushed and concrete crushing initiates at the extreme compressive face of the wall, failure is classified as a CB failure.
  - b) If $\varepsilon_t/\varepsilon_{u,BE} < \varepsilon_{lim}$, the concrete in the vicinity of the extreme compression reinforcing bar has crushed, the concrete at the web-boundary element interface has crushed and concrete crushing initiates at the web-boundary element interface, failure is classified as a CS failure.
  - c) If concrete has crushed and $\varepsilon_t/\varepsilon_{u,BE} > \varepsilon_{lim}$ the solution step at which $\varepsilon_t/\varepsilon_{u,BE} = \varepsilon_{lim}$ is considered. If the concrete was crushed at that point, failure is classified as a CB or CS failure per criteria a) and b) above. If the concrete had not crushed, failure is classified as a BR failure.
- Case 2: ATENA reports a numerical error.
  - a) If $\varepsilon_t/\varepsilon_{u,BE} > \varepsilon_{lim}$ and the concrete has not crushed, then failure is classified as a BR failure.
  - b) If $\varepsilon_t/\varepsilon_{u,BE} < \varepsilon_{lim}$ and the concrete has not crushed, the numerical instability has caused termination of the analysis and the numerical stability of the model must be improved to enable simulation of response out to failure.
  - c) If $\varepsilon_t/\varepsilon_{u,BE} > \varepsilon_{lim}$ and the concrete has crushed, the rules for Case 1 apply.
- Case 3: ATENA does not fail and the load protocol completed successfully.
  - a) If $\varepsilon_t/\varepsilon_{u,BE} > \varepsilon_{lim}$ and concrete has not crushed, a BR failure has occurred.
  - b) If the concrete crushed at an earlier point and load transferred into the compression reinforcement, go back to the point of concrete crushing and apply criteria from Case 1.
  - c) If $\varepsilon_t/\varepsilon_{u,BE} < \varepsilon_{lim}$ and concrete has not crushed, the load protocol must be extended for the specimen to reach failure.

3.3 Comparison of simulated and measured response

ATENA analyses were performed for all of the wall specimens listed in Table 1. Specimen models were subjected to axial load and shear load to replicate the load distribution employed in the laboratory. Lateral load was applied under displacement control. To reduce computational demand, a monotonically increasing, rather than a cyclic, lateral load history was employed. Results of previous research by the authors suggests that stiffness, strength and deformation capacity simulated using a monotonic load history is not significantly different from that simulated using a cyclic history.

Figure 3 shows simulated and measured normalized base shear versus drift at the point of applied lateral load for three specimens exhibiting the three failure modes considered in this study; results in Figure 3 are representative of those for other specimens in the data set. Table 3 list statistics for the dataset for ratios of simulated to measured response quantities. In Table 3, i) yield displacements Δ_{y_sim} and Δ_{y_lab} are, respectively, the simulated and measured lateral displacements at the point of applied lateral load for an applied shear load resulting in extreme reinforcement carrying the yield stress, ii) maximum shear forces V_{max_sim} and V_{max_lab} are, respectively, the simulated and measured maximum shear load carried by the wall, and iii) displacement capacities Δ_{u_sim} and Δ_{yu_lab} are, respectively, the simulated and measured lateral displacements at onset of failure as defined in Section 3.2.

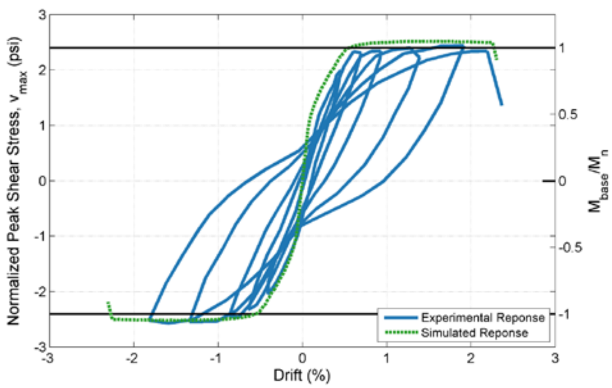

(a) Specimen RW1 (BR failure)

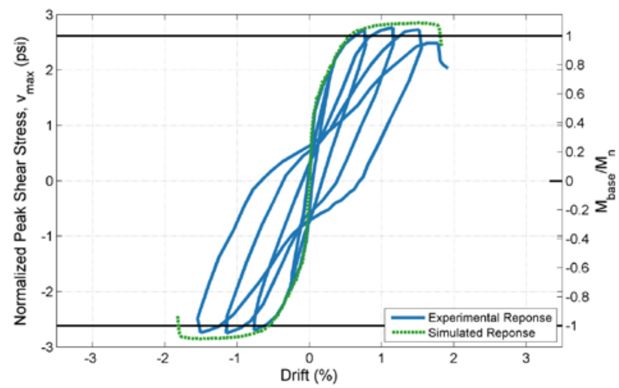

(b) Specimen WSH4 (CB failure)

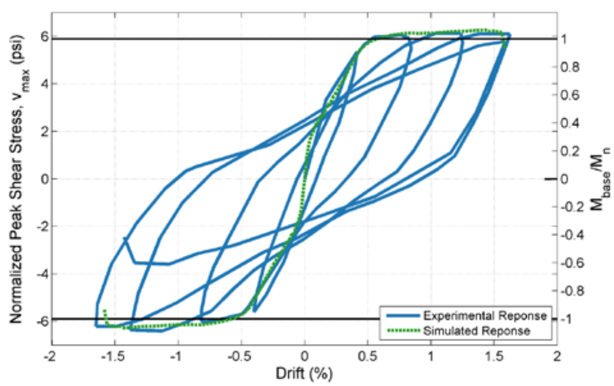

(c) Specimen S6 (CS failure)

Figure 3 – Simulated and measured load versus drift. Base shear is normalized by $\sqrt{f_c'}A_g$ with f_c' in psi. Base moment is normalized by M_n, the nominal flexural strength of the wall defined by per ACI 318-14.

Table 3: Statistics for simulated versus measured response quantities

		$\Delta_{y\_sim}/\Delta_{y\_lab}$	V_{max_sim}/V_{max_lab}	$\Delta_{u\_sim}/\Delta_{u\_lab}$
All Specimens	Mean	0.91	0.99	0.98
	COV	0.29	0.05	0.06
BR Specimens	Mean	0.95	0.98	1.01
	COV	0.31	0.05	0.10
CB Specimens	Mean	0.89	1.01	0.98
	COV	0.20	0.05	0.07

The data presented in Figure 3 and Table 3 show that strength and drift capacity are accurately and precisely simulated. These two quantities are considered to be particularly important for earthquake engineering applications as strength determines the onset of yielding and displacement capacity determines the onset of failure. The data in Figure 3 and Table 3 show also that yield displacement is predicted with much less accuracy and precision. Specifically, yield displacement is underestimated by the ATENA model by as much as 11%, and the COV for yield displacement has a maximum value of 30%. Here it should be noted that uncertainty in yield displacement is due primarily to specimen R1; if specimen R1 is removed from the data set the COV for prediction of yield displacement is reduced to 0.17. Underestimation and imprecision of simulated yield displacement is attributed to the fact that shrinkage cracking is not simulated and that stiffness loss due to shrinkage cracking can be significant [15]. Underestimation of yield displacement for laboratory wall specimens is common.

3.4 Simulation results for walls exhibiting different failure mechanisms in the laboratory

Beyond providing simulation of global response quantities, such as load-displacement response, continuum-type analysis also provides simulation of local response quantities, such as stress and strain. For all of the specimens listed in Table 1, stress and strain fields were investigated. Minimum principal stress fields were found to be particularly valuable for understanding response mechanisms and failure modes. The data in Figure 4 show minimum principal stress fields for walls exhibiting BR (left), CB (middle) and CS (right) failure modes at nominal flexural strength (top) and onset of strength loss (bottom). In this figures red and yellow correspond to small negative (compressive) principal stresses and green and blue correspond to large negative (principal) stress. In this figure, vertical black lines indicate the interface between the heavily reinforced, confined boundary element and the lightly reinforced web region of the wall. The data in Figure 4 show the following:

- Walls with high shear stress demands, such as wall specimen S6, develop large negative principal stresses within the web of the wall and at the boundary element interface.
- At nominal flexural strength, M_n, (top row) walls show a relatively linear principal stress distribution within the boundary element. All walls, regardless of failure mechanism, show minimum principal stresses at the extreme compression fiber, with minimum principal stress diminishing towards web of the wall.
- At onset of failure (bottom row), different failure modes show different patterns of concrete crushing. Note that crushed concrete is concrete that carries large compressive stresses at M_n (green or blue in top row) and low compressive stresses at onset of failure (yellow or red in bottom row).
- For walls exhibit a BR failure, concrete crushing is limited to the extreme concrete compression fibers. For wall exhibiting a CB failure, most of the boundary element concrete crushes. For walls exhibiting CS failure, all of the boundary element concrete crushes with maximum strength loss occurring at the interface between the boundary element and the web.

Taken together, the above observations suggest that in walls with high shear stress demands, minimum principal stresses resulting from shear and flexural response modes combine to result in maximum compression demands and concrete crushing occurring at the interface between the boundary element and the web.

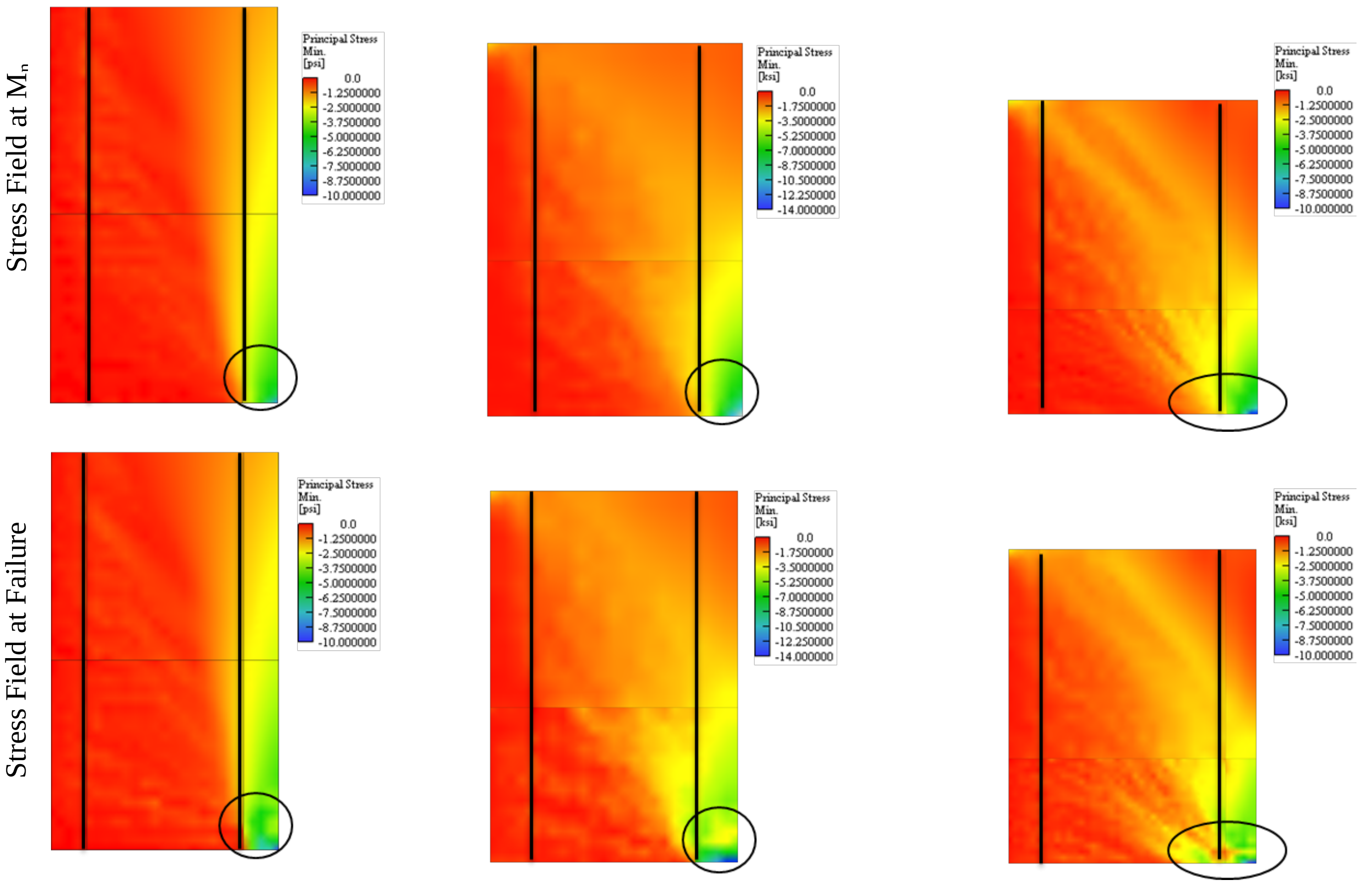

(a) RW1 (BR Failure) (b) RW-A20-P10-S63 (CB Failure) (c) S6 (CS Failure)

Figure 4: Simulated minimum principal stress fields at nominal flexural strength, M_n, (top row) and at onset of failure (bottom row) for specimens exhibiting BR, CB and CS failure modes

4. Investigation of wall failure mechanisms and deformation capacity using ATENA

The data in Figure 3 suggest that the deformation capacity of walls is a function of shear demand and cross-sectional aspect ratio and, to some extent, axial load ratio. Evaluation of the nonlinear continuum-type model shows that the ATENA model can provide accurate simulation of drift capacity and failure mechanism. Thus, a simulation-based parameter study was undertaken to improve understanding of wall drift capacity and the design parameters that determine failure mode and drift capacity. A series of approximately 60 wall specimens were design to achieve flexure-controlled response with 1) shear stress demand varying from $2\sqrt{f_c'}A_g$psi to $10\sqrt{f_c'}A_g$psi with f_c' in psi $\left(0.17\sqrt{f_c'}A_g \text{ MPa to } 0.83\sqrt{f_c'}A_g \text{ MPa with } f_c' \text{ in MPa}\right)$and 2) CSAR varying from 8 to 20. Longitudinal reinforcement ratio, axial load ratio and shear span were varied to achieve the desired range of shear stress demand. Walls were subjected to constant axial load and monotonically increasing lateral loading applied under displacement control.

For each specimen in the parameter study, failure modes defined per Section 3.2 and drift capacity were recorded. Results of the parameter study are presented in Figure 5 and Figure 6. In Figure 5, $v_{max} = V_{max}\sqrt{f_c'}A_g$, where V_{max} is the maximum shear force carried by the wall, f_c' is concrete compressive strength in psi, and $A_g$is the cross-sectional area of the wall. Data in these figures show the following:

- Walls with larger CSAR and higher shear demands are more likely to develop a CS failure mode, for which failure initiates with crushing of concrete at the boundary element-web interface.

- Walls with lower CSAR and lower shear stress demands develop CB and BR failure modes, for which failure results from fracture of previously buckled reinforcement (BR) or simultaneous crushing of concrete and buckling of longitudinal reinforcement (CB).
- The drift capacity of walls exhibiting CS failure is substantially less than that of walls exhibiting a BR or CB failure.
- The drift capacity of walls exhibiting BR and CB failures is approximately the same.

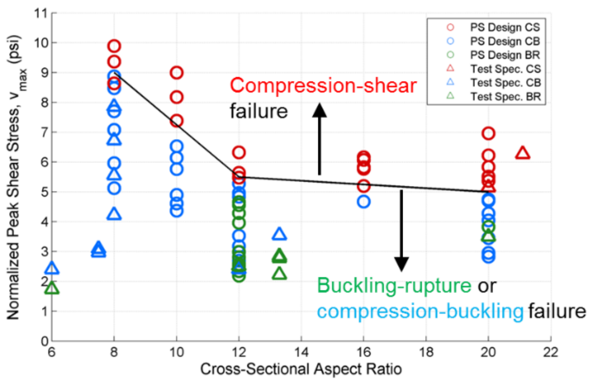

Figure 5 – Failure mode as a function of normalized shear demand and CSAR.

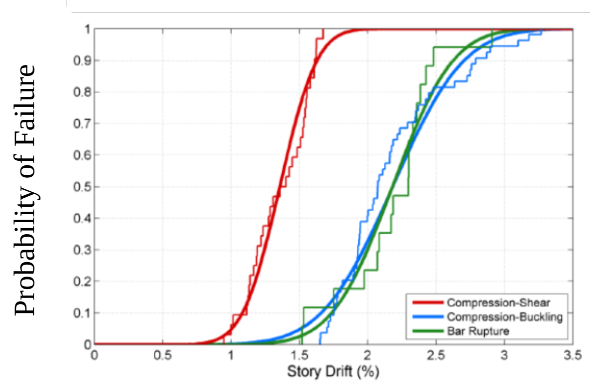

Figure 6 – Failure mode as a function of normalized shear demand and CSAR

5. Summary and Conclusions

Data from previous laboratory tests of reinforced concrete walls suggest that the deformation capacity of slender planar concrete walls is determined primarily by shear stress demand, cross sectional aspect ratio and axial load ratio. Nonlinear finite element analysis was used investigate wall response and the mechanisms by which these design parameters determine deformation capacity under lateral loading. The ATENA software package was employed with concrete modeled using solid elements, steel modeled using line elements, and the assumption of perfect concrete-steel bond. The ATENA model was calibrated using data from 23 experimental tests of planar concrete walls with a range of design parameters and subjected to cyclic lateral loading and constant axial loading. The calibrated model provides accurate and precise simulation of strength and deformation capacity (maximum error of 2% and COV of 10%) and moderately accurate and precise simulation of yield displacement (maximum error of 11% and COV of 17% when one outlier was removed from the data set). Using the calibrated model, simulations were completed of a series of planar walls with a range of cross-sectional aspect ratios, shear stress demands and axial load ratios. The results of these analyses show that 1) shear stress demand and cross-sectional aspect ratio are the primary variables determining failure mode and deformation capacity; axial load primarily acts to increase flexural capacity and, as a result, shear demand, 2) walls with large cross-sectional aspect ratios and high shear demands may exhibit compression-shear failure characterized by crushing of concrete at the web-boundary element interface, 3) the deformation capacity of walls exhibiting a compression-shear failure is much less than that of walls exhibiting a compression-buckling or buckling-rupture failure mechanism, and 4) the deformation capacity of walls exhibiting compression-buckling or buckling-rupture failures is approximately the same.

6. Acknowledgements

The work forming the basis for this publication was conducted pursuant to a contract with the Federal Emergency Management Agency. The substance of such work is dedicated to the public. The authors are solely responsible for the accuracy of statements or interpretations contained in this publication. No warranty is offered with regard to the results, findings and recommendations contained herein, either by the Federal Emergency Management Agency, the Applied Technology Council, its directors, members, or employees. These

organizations and individuals do not assume any legal liability or responsibility for the accuracy, completeness, or usefulness of any of the information, product or processes included in this publication.

7. References

[1] Birely AC (2012). "Seismic Performance of Slender Reinforced Concrete Structural Walls" *PhD Dissertation*. University of Washington, Seattle.

[2] Whitman Z (2015). "Investigation of Seismic Failure Modes in Flexural Concrete Walls Using Finite Element Analysis." *MS thesis*, University of Washington, Seattle.

[3] Pugh JS (2012). "Numerical Simulation of Walls and Seismic Design Recommendations for Walled Buildings." *PhD Dissertation*. University of Washington, Seattle.

[4] ACI (2014). *Building Code Requirements for Structural Concrete (ACI 318-14) and Commentary on Building Code Requirements.* American Concrete Institute.

[5] Dazio A, Beyer K, Bachmann H (2009). "Quasi-Static Cyclic Tests and Plastic Hinge Analysis of RC Structural Walls." *Engineering Structures* 31 (7): 1556–71. doi:10.1016/j.engstruct.2009.02.018.

[6] Liu, H. 2004. "Effect of Concrete Strength on the Response of Ductile Shear Walls." *MS thesis*, Montreal, QB: Dept. of Civil Engineering and Applied Mechanics, McGill University.

[7] Lowes, L.N., Lehman, D.E., Birely, A.C., Kuchma, D.A., Marley, K.P., Hart, C.R. "Earthquake Response of Slender Planar Concrete Walls with Modern Detailing" *Engineering Structures* Vol. 43, (2012).

[8] Thomsen J, Wallace J (2004). "Displacement-based design of slender reinforced concrete structural walls – experimental verification," *Journal of Structural Engineering, ASCE* 130(4): 618–630.

[9] Vallenas J, Bertero VV, Popov E (1979). "Hysteretic behavior of reinforced concrete structural walls," Earthquake Engineering Research Center, Berkeley, CA, Tech. Rep. No. UCB/EERC-79/20.

[10] Oh, Young-Hun, Sang Whan Han, and Li-Hyung Lee. 2002. "Effect of Boundary Element Details on the Seismic Deformation Capacity of Structural Walls." *Earthquake Engineering & Structural Dynamics* 31 (8): 1583–1602. doi:10.1002/eqe.177.

[11] Oesterle, R., A. Aristizabal-Ochoa, J. Carpenter, H. Russell, and W. Corley. 1976. "Earthquake resistant structural walls - tests of isolated walls," *Portland Cement Association/National Science Foundation, Washington, D.C., Tech. Rep. No. NSF/RA-760815*.

[12] Tran, Thien Anh. 2012. "Experimental and Analytical Studies of Moderate Aspect Ratio Reinforced Concrete Structural Walls." Ph.D. dissertation, Los Angeles, CA: Dept. of Civil and Environmental Engineering, University of California, Los Angeles.

[13] Červenka V, Jendele L, Červenka J (2014). *ATENA Program Documentation Part 1: Theory*. Červenka Consulting.

[14] Menetrey, P., and William, K.J. 1995. "Triaxial Failure Criterion for Concrete and Its Generalization." *ACI Structural Journal* 92 (3). doi:10.14359/1132.

[15] Pallermo D, Vecchio FJ (2007). "Simulation of Cyclically Loaded Concrete Structures Based on the Finite Element Method" *Journal of Structural Engineering, ASCE* 133(5): 728-738.